

Two energy scales and two distinct quasiparticle dynamics in the superconducting state of underdoped cuprates

M. LE TACON^{1,2*}, A. SACUTO^{1,2}, A. GEORGES³, G. KOTLIAR^{3,4,5}, Y. GALLAIS⁶, D. COLSON⁷ AND A. FORGET⁷

¹Laboratoire Matériaux et Phénomènes Quantiques (UMR 7162 CNRS), Université Paris 7, 2 place Jussieu 75251 Paris, France

²Laboratoire de Physique du Solide, ESPCI, 10 rue Vauquelin 75231 Paris, France

³Centre de Physique Théorique, Ecole Polytechnique, 91128 Palaiseau Cedex, France

⁴Service de Physique Théorique, CEA-Saclay, 91191 Gif-sur-Yvette, France

⁵Serlin Physics Laboratory, Rutgers University, USA

⁶Departments of Physics and Applied Physics, Columbia University New York, New York 10027, USA

⁷Service de Physique de l'Etat Condensé (CNRS URA 2464), DSM/DREGAM/SPEC, CEA Saclay, 91191 Gif-sur-Yvette Cedex, France

*e-mail: mathieu.le-tacon@espci.fr

Published online: 23 July 2006; doi:10.1038/nphys362

The superconducting temperature T_c of hole-doped high-temperature superconductors has a dome-like shape as a function of hole concentration, with a maximum T_c at 'optimal' doping. On the underdoped side, the superconducting state is often described in terms of one energy scale, associated with the maximum of the d -wave gap (at the antinodes), which increases as the doping decreases. Here, we report electronic Raman scattering experiments that show a second energy scale in the gap function: the slope of the gap at the nodes, which decreases with decreasing doping. Our measurements also reveal two distinct quasiparticle dynamics; electronic coherence persists down to low doping levels at the nodes, whereas antinodal quasiparticles become incoherent. Using a sum-rule, we find that the low-frequency Raman response and the temperature dependence of the superfluid density, both controlled by nodal excitations, behave in a qualitatively similar manner with doping variation.

There is now consensus that the 'normal state' above T_c in the underdoped and optimally doped regimes is far from normal.

In particular, a pseudogap develops in the underdoped regime, corresponding to a partial suppression of spin and charge excitations. This phenomenon lies outside the standard theory of solids and manifests itself in several experiments¹.

In contrast, there is no consensus on whether the superconducting state in the underdoped regime, which emerges from the Mott insulating state, can be described by the standard Bardeen, Cooper and Schrieffer (BCS) theory, or its strong coupling Migdal–Eliashberg extension, for a d -wave superconductor. In this article, we address this issue using electronic Raman spectroscopy (ERS). ERS is a powerful tool for probing quasiparticles of the superconducting state in selected parts of momentum space, namely the antinodal (ANR) and nodal (NR) regions, where the amplitude of the superconducting gap reaches its maximum and vanishes respectively². Here ERS measurements have been carried out on selected as-grown $\text{HgBa}_2\text{CuO}_{4+\delta}$ (Hg-1201) single crystals with different doping levels extending from the slightly overdoped to the underdoped regime (see the Methods section). Hg-1201 has one of the simplest structures, with only one CuO_2 plane per unit cell and a pure tetragonal symmetry. Whereas most of the previous work was done either on $\text{YBa}_2\text{Cu}_3\text{O}_{7+\delta}$ (Y-123) or $\text{Bi}_2\text{Sr}_2\text{CaCu}_2\text{O}_{8+\delta}$ (Bi-2212) which exhibited a small orthorhombic distortion, the tetragonal Hg-1201 system allows us to separately measure pure nodal and antinodal responses, without mixing effects. Our results demonstrate that the superconducting state on the underdoped side is also not normal, and cannot be described within the standard d -wave BCS model. We show that the superconducting order parameter is controlled by two parameters (the slope of the gap at the nodes and its maximum amplitude at the antinodes) with distinct dependences on doping,

instead of only one as expected from a standard d -wave gap. We find a strong momentum dependence of the quasiparticle spectral weight (QPSW) in the superconducting state of the underdoped regime, and we finally establish, using a new Raman sum rule, a relationship between the superfluid density and the low-energy Raman scattering associated with nodal physics, suggesting that the Fermi-liquid renormalization of the current and Raman tensor (which transforms as a product of currents) have similar doping dependence. Our new experimental results place strong constraints on theories of the high-temperature superconductivity phenomenon.

EXPERIMENTAL RESULTS

Figure 1 shows the NR and ANR Raman responses in both the normal and superconducting states of the Hg-1201 single crystals, at various doping levels. At optimal doping ($T_c = 95$ K), the electronic Raman continua for both the NR and ANR exhibit a redistribution of spectral weight from energies lower than 400 cm^{-1} to higher energy, when going from the normal to the superconducting state. At low energy (below 400 cm^{-1}), the ANR superconducting continuum exhibits a cubic frequency dependence with a well-marked superconducting pair-breaking peak, at a frequency $\omega_{AN} \simeq 505\text{ cm}^{-1}$ ($\simeq 8k_B T_c$, where k_B is the Boltzmann constant). In contrast, the superconducting spectrum in the NR has a linear frequency dependence up to 400 cm^{-1} , as well as a weaker signature of the pair-breaking peak close to the same frequency $\omega_N \simeq \omega_{AN}$ that for the ANR spectrum.

The Raman response at optimal doping is thus characterized by a single energy scale $\omega_{AN} \simeq \omega_N$ associated with the pair-breaking peak, and all the features described above are consistent with those expected for a d -wave superconductor² with a maximum value Δ_m of the superconducting gap given by $2\Delta_m = \omega_{AN}$. Our results for one overdoped sample (spectra at the top of Fig. 1) can also be interpreted in terms of a single energy scale.

In contrast, as doping is decreased below the optimal level, the evolution of the Raman spectra in the superconducting phase becomes strikingly different in the ANR and in the NR. As the doping level (and T_c) is reduced, the energy of the antinodal peak (indicated by an arrow on the right panel of Fig. 1) increases. Simultaneously, the intensity of this peak rapidly decreases as T_c decreases, and finally disappears in the vicinity of $T_c = 78$ K. On the contrary, the nodal peak persists down to the lowest doping that we have studied ($T_c = 63$ K), and its energy follows T_c . We note that similar observations have been reported previously for other cuprates, such as Y-123, Bi-2212, $\text{Bi}_2\text{Sr}_{2-x}\text{La}_x\text{CuO}_{6+\delta}$ (Bi-2201) and $\text{La}_{2-x}\text{Sr}_x\text{CuO}_4$ (LSCO)³⁻⁵. This demonstrates that the electronic Raman response in the underdoped regime involves two distinct energy scales, with opposite doping dependences. As discussed below, this is inconsistent with a simple BCS d -wave description².

To further substantiate this point, in Fig. 2 we have plotted the characteristic ratios $\omega_{AN}/T_c^{\text{max}}$ and $\omega_N/T_c^{\text{max}}$ obtained for several families of cuprates by different groups³⁻⁵, as a function of doping at a fixed temperature well below T_c (T_c^{max} is T_c at optimal doping). The doping value p is inferred from T_c using Tallon's equation⁶: $1 - T_c/T_c^{\text{max}} = 82.6(p - 0.16)^2$. Figure 2 reveals that these ratios have a universal dependence on doping. For underdoped compounds, two distinct scales are present, clearly separated beyond the scatter of the data, with the two ratios behaving in opposing ways as a function of doping, whereas a unique energy scale (and doping dependence) is recovered in the optimally doped and overdoped regime.

We do not address the more subtle effects here, such as the possible downwards shift of the higher-energy scale in Raman measurements, due to collective modes⁷.

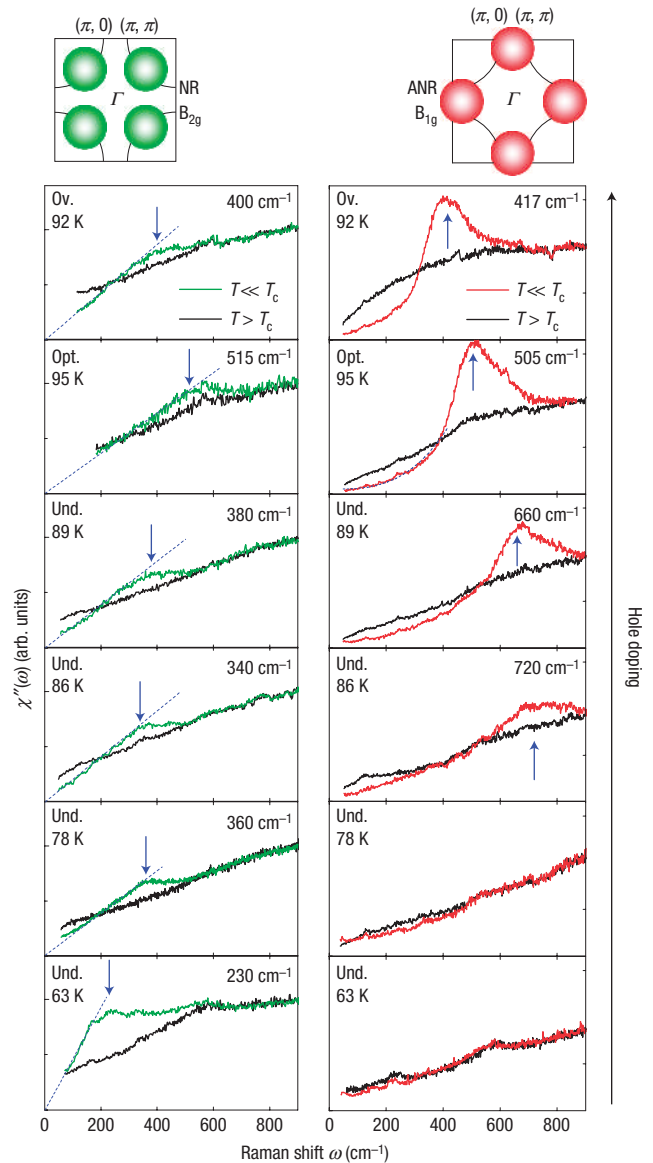


Figure 1 Raman responses in the nodal (B_{2g}) and antinodal (B_{1g}) regions as a function of doping. The dashed lines on B_{2g} (B_{1g}) spectra show the linear (cubic) frequency dependences of the nodal (antinodal) Raman responses. The arrows indicate the position of the superconducting peak maxima. We clearly distinguish two energy scales that depend on doping in opposite directions. Ov.: overdoped; Opt.: optimally doped; Und.: underdoped.

INCONSISTENCY WITH A SIMPLE BCS MODEL

Let us now analyse these results using the simplest possible framework, that of a BCS superconductor with a d -wave gap function of the form $\Delta_{\mathbf{k}} = \Delta_m \cos(2\phi)$ (ϕ is the angle associated with momentum \mathbf{k} on the Fermi-surface). The Raman response would then read^{2,8}:

$$\chi''_{AN,N}(\omega) = \frac{2\pi N_F}{\omega} \text{Re} \left\langle \frac{(\gamma_k^{AN,N}(\phi))^2 \Delta_m^2 \cos^2(2\phi)}{\sqrt{\omega^2 - 4\Delta_m^2 \cos^2(2\phi)}} \right\rangle_{\text{FS}} \quad (1)$$

where N_F is the density of states at the Fermi level, $\gamma_k^{AN,N}(\phi)$ is the Raman vertex associated with each polarization:

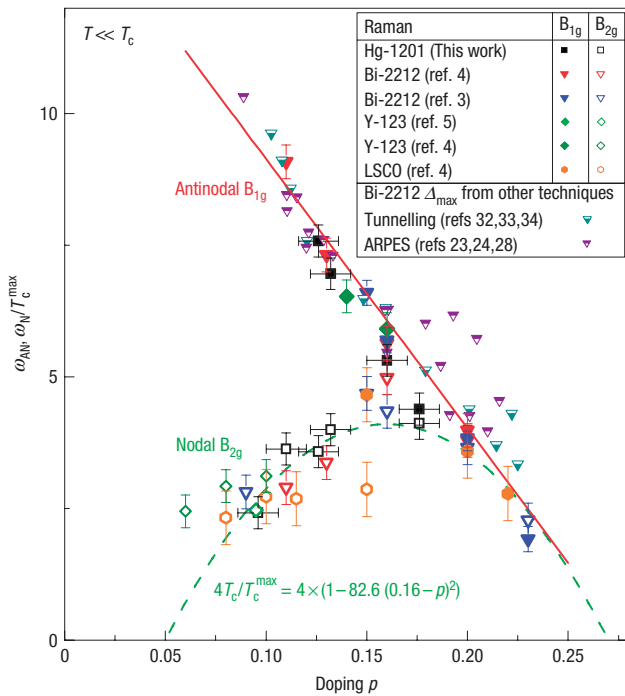


Figure 2 Universal doping dependence of the ratios ω_{AN}/T_c^{\max} and ω_N/T_c^{\max} of the antinodal (B_{1g}) and nodal (B_{2g}) superconducting peaks (obtained from Hg-1201 (this work), Bi-2212 in refs 3,4, Y-123 in refs 4,5 and LSCO in ref. 4).

The error bars on the B_{1g} and B_{2g} Raman peak locations have also been reported and show unambiguously that there are two energy scales in the underdoped side of hole-doped cuprates. The ratios $2\Delta/T_c^{\max}$ deduced from ARPES coherent peak in the antinodal region^{23,24,28} and from tunnelling spectroscopy^{32–34} are plotted.

$\gamma^{AN}(\phi) = \gamma_{B_{1g}} \cos(2\phi)$ whereas $\gamma^N(\phi) = \gamma_{B_{2g}} \sin(2\phi)$, and $\langle \dots \rangle_{FS}$ denotes a Fermi-surface average. This predicts a sharp pair-breaking peak (corresponding to a divergence of this expression) in the ANR (B_{1g} geometry) at $\omega = 2\Delta_m$, and a weaker singularity in the NR (B_{2g}) at the same frequency scale. Furthermore, within the BCS formula above, the NR response has a maximum at a somewhat lower energy than the peak in the ANR, but both are governed by one energy scale, that of the maximal gap Δ_m .

Inclusion of damping parameters² in equation (1) and a more realistic description of the doping dependence of the Fermi surface introduces minor changes and fails to reproduce the opposite doping dependence of the antinodal and nodal peaks.

This clearly demonstrates that one or both of the following assumptions become invalid in the underdoped regime: (1) non-interacting BCS quasiparticles (2) a gap function with the simple form $\Delta_k = \Delta_m \cos(2\phi)$ characterized by a single energy scale. Moving away from assumption (1) requires taking into account, in the framework of the Landau theory of interacting quasiparticles, the spectral weight Z_k of these quasiparticles, smaller than one and k -dependent, as well as the Fermi-liquid vertex Λ_k describing the interaction of the quasiparticles with external perturbations. This leads to (see the Methods section):

$$\chi''_{AN,N}(\omega) = \frac{2\pi N_F}{\omega} \text{Re} \left\langle \frac{(Z\Lambda)_k^2 (\gamma_k^{AN,N})^2 \Delta_k^2}{\sqrt{\omega^2 - 4\Delta_k^2}} \right\rangle_{FS} \quad (2)$$

in which a general gap function has also been taken into account. This expression contains two unknown functions of momentum

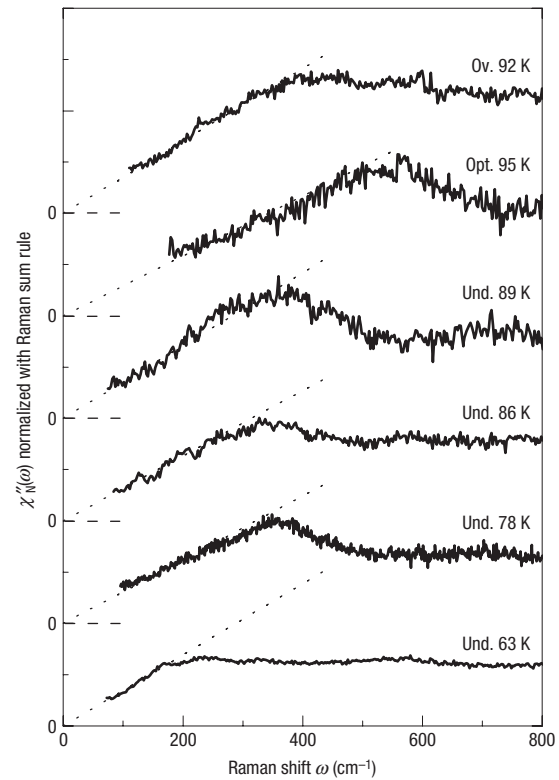


Figure 3 Normalized Raman response functions with respect to the sum rule.

A weak linear background coming from spurious luminescence for intermediate doping, independent of the scattering geometry and excitation lines, has been subtracted from raw data before carrying out the normalization (note that without this subtraction the final result is qualitatively similar, that is, the low-energy slope α of the normalized nodal Raman response is found to be doping independent).

on the Fermi surface: $(Z\Lambda)_k$ and Δ_k , the determination of which requires further considerations.

LOW-ENERGY NODAL EXCITATIONS

To gain such insight, we focus on the low-energy part of the Raman spectra, which is controlled by the properties of nodal quasiparticles. The B_{2g} geometry is particularly significant in this respect, because it directly probes the NR (see the Methods section). Figure 1 demonstrates that a linear dependence on frequency is found in this geometry, for all doping levels. This is expected from equation (2), which yields: $\chi''_N(\omega \rightarrow 0) = \gamma_{B_{2g}}^2 (\pi^2 N_F / 2\nu_\Delta) (Z\Lambda)_N^2 \omega + \dots$. In this expression, $\nu_\Delta = (d\Delta/d\phi)|_N$ is the slope of the gap function at the nodes, and $(Z\Lambda)_N$ is the value of $(Z\Lambda)_k$ at the node. Hence, in principle, a study of the doping dependence of the term linear in frequency in the (B_{2g}) response enables the determination of the important parameter:

$$\alpha \equiv \frac{N_F}{\nu_\Delta} (Z\Lambda)_N^2 \quad (3)$$

associated with nodal low-energy physics. To compare this parameter for different samples, the Raman spectra must be properly normalized. In this paper, we do not present absolute Raman cross-sections because (1) the Raman intensity is sensitive to the surface topology and we measured a different crystal for

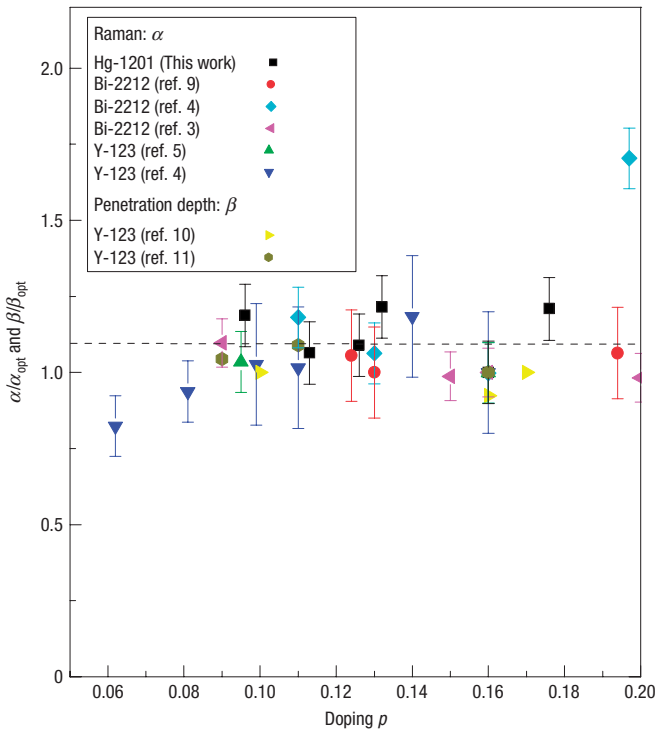


Figure 4 Doping dependence of the low-energy slope α of the nodal (B_{2g}) Raman response ($\alpha = (N_F / v_\Delta)(Z\Lambda)_N^2$), normalized to the optimal doping one ($p = 0.16$). The error bars originate from the linear fitting of this slope from our data and those of refs 3–5,9. The Fermi-liquid parameter $\beta = (N_F / v_\Delta)(Z\Lambda)_N^2$ extracted from the temperature dependence of the penetration depth^{10,11}, is also shown. α and β are both found to be doping independent in the range ($p = 0.09$ – 0.020).

each doping and (2) it is difficult to obtain the complex refractive indices by ellipsometry measurements due to the small size of Hg-1201 crystals. As absolute measurements are not available, we have normalized the spectra using a theoretical sum rule that we have established for the Raman intensity of a weakly doped Mott insulator. This sum rule reads, at low doping levels p : $\int_0^\Omega \chi''(\omega)\omega d\omega = Cp$. We have derived this expression (see the Methods section) by starting from a one-band t – J model, in which case the upper cutoff Ω can be taken to infinity, and the constant C depends on the hopping amplitudes and exchange constant: $C(t, t', J)$. We expect this expression to be general for a weakly doped Mott insulator, provided the upper cutoff is taken to be smaller than the bare bandwidth, and much smaller than the Mott or charge-transfer gap. We have normalized our Raman B_{2g} responses using this sum rule. This is shown in Fig. 3, and reveals that in the doping range of interest the low-energy linear term of the B_{2g} Raman response (normalized using the sum rule) is doping independent. To demonstrate the universality of this phenomenon, we have applied the same sum rule to previous Raman spectra of Y-123 and Bi-2212^{3–5,9}. The results are shown in Fig. 4. It is seen that the low-energy parameter α associated with the ω -linear term of the B_{2g} Raman response is essentially doping independent for all doping levels between $p = 0.16$ down to $p = 0.09$. For smaller doping levels, the Y-123 data (two points available) suggest that α may end up decreasing.

This doping independence of the Raman B_{2g} (NR) slope over an extended range of doping levels is reminiscent of the behaviour of the slope β of the linear term in the temperature dependence of

the penetration depth (or superfluid density)^{10,11}: $\rho_s(T) = \rho_s(0) - \beta T + \dots$. This quantity is also associated with the physics of nodal quasiparticles, and is given by almost the same expression^{12–14} $\beta \propto (v_F / v_\Delta)(Z\Lambda)_N^2$, except for the fact that the Fermi-liquid parameter Λ_ρ corresponds to a different angular-momentum channel to that in the Raman case. The comparison made in Fig. 4 between these two quantities shows excellent agreement, hence establishing a previously unforeseen relation between Raman and penetration depth measurements. We also note that recent experiments¹⁵ suggest deviations from $\beta = \text{const.}$ at very low doping levels, in agreement with the two highly underdoped Y-123 data points in Fig. 4. As pointed out in ref. 12, the independence of the slope β of the superfluid density on doping, in an extended range, is a serious difficulty for the simplest (‘vanilla’) version of the resonating valence bond theory¹⁶, in either its auxiliary boson¹⁷ or wavefunction formulations^{18,19}. Our observations reveal a similar problem in connection with Raman scattering.

Having established the doping (in)dependence of the α parameter associated with nodal physics, we can make further progress in disentangling the relative effects of (1) quasiparticle dynamics and (2) the form of the gap function on the Raman spectra. Let us first assume that the gap function has the simple form: $\Delta_k = \Delta_m \cos(2\phi)$ characterized by a single energy scale (Δ_m), and such that $v_\Delta = 2\Delta_m$. As the behaviour of the ANR (B_{1g}) peak implies that Δ_m increases as doping is reduced (Fig. 2), the doping independence of α would then imply that $(Z\Lambda)_N$ must correspondingly increase as p is reduced. This behaviour is highly unlikely to apply for a doped Mott insulator, because it would correspond to a reinforcement of the QPSW as doping is reduced. Furthermore, angle-resolved photoemission spectroscopy (ARPES) data and theory do suggest that the nodal QPSW decreases as p is reduced^{20,21}. Hence, we are led to suspect that the slope of the gap at the nodes, v_Δ , must decrease as the doping level is reduced (to keep α constant) and hence does not track the maximum gap Δ_m . This has far-reaching consequences, namely: (1) that a pure $\cos(2\phi)$ form does not hold in the underdoped regime, and (2) that two energy scales characterize this regime (as already foreseen from the analysis in Fig. 2). Indeed, this has previously been suggested from ARPES experiments^{22,23}, indicating that the superconducting gap function may change from a ‘V-shape’ to a ‘U-shape’ as the doping level is reduced.

PHENOMENOLOGICAL DESCRIPTION

We now return to the general expression for the Raman response based on Fermi-liquid considerations, and explore whether reasonable momentum and doping dependence of the two functions $(Z\Lambda)_k$ and Δ_k (associated with quasiparticle physics and the superconducting gap, respectively) can describe our data. We use the shape of the gap function (consistent with d -wave symmetry) proposed from ARPES data in ref. 22: $\Delta_k = \Delta_m (B \cos 2\phi + (1 - B) \cos 6\phi)$, where $0 \leq B \leq 1$ (see Fig. 5a). This form is characterized by two scales: the (antinodal) maximum gap Δ_m and the nodal slope $v_\Delta = \Delta_m(8B - 6)$. The parameters Δ_m and B were varied, as in ref. 22. First, we found that taking a momentum-independent $Z\Lambda$ was insufficient to account for experimental observations (the maximum of the nodal response does not recede towards lower energy). Hence, a variation of $Z\Lambda$ along the Fermi surface is needed. We have chosen $(Z\Lambda)_k = \sqrt{v_\Delta} \times (1 - C \cos^2(2\phi))$ where $0 \leq C \leq 1$ (chosen in such a way that $(Z\Lambda)_N^2 / v_\Delta$ is kept constant, for consistency with our experimental observation on the doping independence of α) describes the anisotropy of the QPSW. This expression is consistent with doping-dependent spectral weight obtained from ARPES²¹. It is shown in Fig. 5b. The four curves are supposed to correspond, qualitatively,

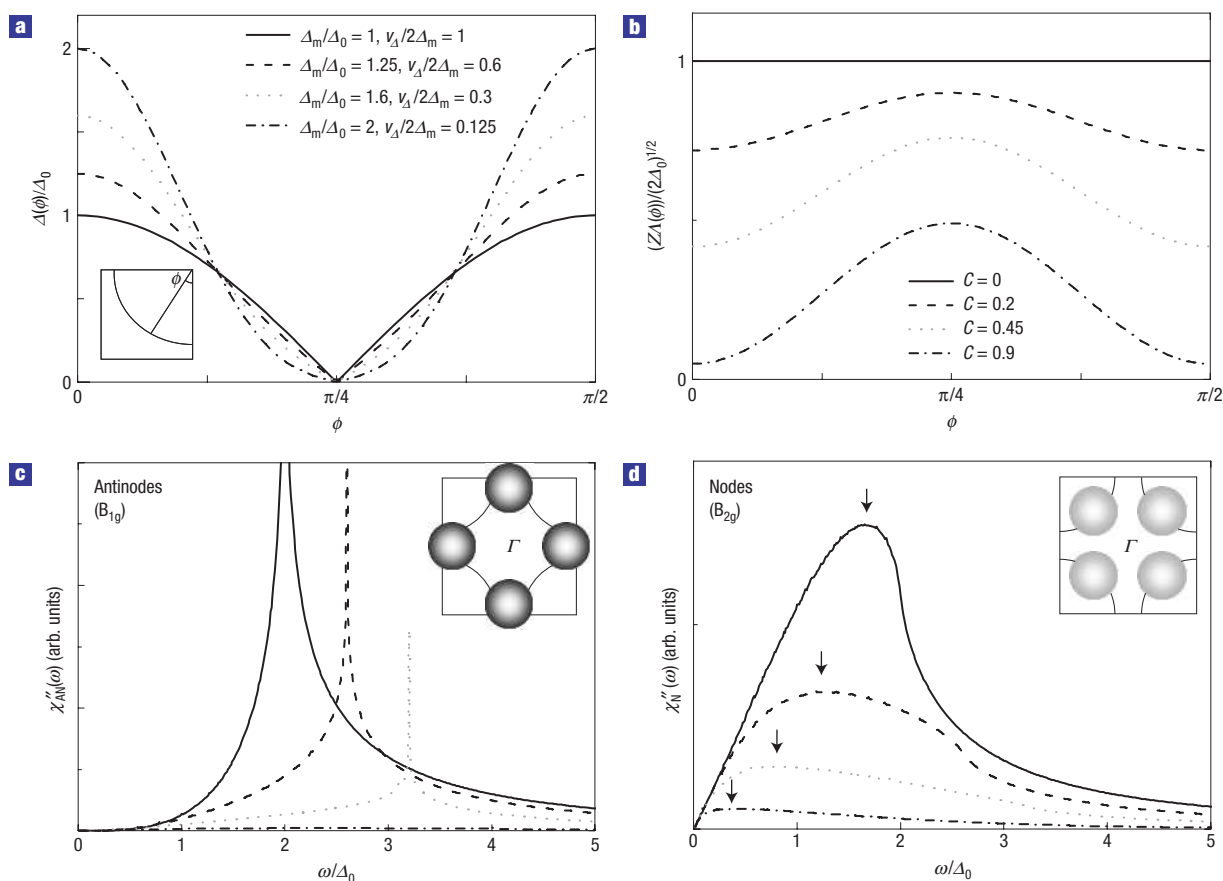


Figure 5 Phenomenological description of the Raman response of underdoped cuprates. **a**, Angular dependence of the phenomenological superconducting gap $\Delta_{\mathbf{k}} \equiv \Delta(\phi)$ as a function of doping. Δ_m stands for the maximum gap amplitude at the antinodes, and Δ_0 is its value for a slightly overdoped Hg-1201. $(v_{\Delta}/2\Delta_m)$ describes the slope of the superconducting gap at the nodes. Both Δ_m and v_{Δ} are doping dependent. **b**, Angular dependence of the phenomenological QPSW $(ZA)_{\mathbf{k}} \equiv ZA(\phi)$. C is doping dependent and describes the anisotropy of the QPSW. **c, d**, Calculated antinodal and nodal Raman responses in the superconducting state using the parameters described in (a) and (b).

to the overdoped (BCS), optimally doped, slightly and strongly underdoped regimes. The resulting spectra are shown in Fig. 5c,d for both ANR (B_{1g}) and NR (B_{2g}). All the main qualitative aspects of our experimental observations are captured by this simple phenomenological model, namely: (1) the opposite variation of the nodal and antinodal peak energies with doping, which implies that the slope of the superconducting gap at the nodes v_{Δ} decreases as the doping is reduced whereas the maximum gap amplitude Δ_m increases at the antinodes, (2) the doping independence of the low-energy parameter α associated with the ω -linear term in the B_{2g} response and (3) the drastic suppression of the antinodal peak due to the loss of coherence of the antinodal quasiparticles, consistent with Fermi-surface ‘arcs’²⁴. Aspects of this phenomenological description emerge from models describing the competition of superconductivity with alternative forms of long-range order^{25–27}. We emphasize, however, that we only observe the nodal and antinodal Raman peaks below T_c .

COMPARISON WITH OTHER EXPERIMENTS

Finally, we discuss whether other experimental probes support the existence of two energy scales (corresponding to the maximum and the nodal slope of the gap) in the superconducting state of the underdoped cuprates.

Let us first note that the two basic building blocks of the phenomenological analysis developed above are consistent with available information from ARPES. The leading edge in the ANR (corresponding to the higher-energy scale) was shown to increase as the doping level was reduced^{28,29}. Evidence for a second energy scale associated with the nodal region, and varying in an opposite manner with doping, has been suggested from ARPES in refs 22,23, with a corresponding change in the gap function as discussed above. More extensive ARPES studies of the leading edge in the NR are clearly needed. ARPES also reveals that the antinodal quasiparticles in the superconducting state quickly lose spectral weight and eventually become incoherent as doping is reduced^{21,29}, whereas nodal quasiparticles lose spectral weight as doping is reduced but maintain coherence down to low doping levels^{20,21}.

It was suggested from thermal conductivity measurements on Y-123³⁰ that the nodal slope of the gap, v_{Δ} , increases as the doping level is reduced, which would seem in contradiction with our observations. However, closer examination reveals that only one data point is available in the doping range of interest here, and more experiments are clearly needed.

Tunnelling, although not a momentum-selective probe like Raman or ARPES, exhibits a set of distinct superconducting line shapes as a function of doping. The main peak in these spectra moves to higher energies as doping is reduced from optimal

doping³¹ (as also seen from break-junction measurements^{32–34}), and at the same time broadens considerably. This is consistent with the behaviour of the higher-energy scale, and with the rapid loss of coherence of antinodal quasiparticles. Fourier-transform tunnelling has shown that antinodal decoherence is closely related to a local charge order, at least in the surface³¹. This is consistent with the loss of the electronic Raman response that is sensitive to the charge dynamics. In contrast, the observation of quasiparticle interferences from tunnelling³⁵ provides strong evidence for the coherence of nodal quasiparticles. There are also some previous and recent indications that the lower-energy scale might show up as the gap edge in the Andreev reflection spectra³⁶ and a low-voltage shoulder in the tunnelling spectra of underdoped samples³¹.

CONCLUSION

In summary, ERS clearly demonstrates the existence of two distinct energy scales in the superconducting state of underdoped cuprates, with opposite doping dependence. Here, we have suggested that these two scales are associated with the nodal slope of the gap function, v_{Δ} , and its maximum Δ_m , respectively. v_{Δ} decreases whereas Δ_m increases as the doping decreases. Correspondingly, our experiments reveal two different dynamical properties of the quasiparticles in these two regions. Hence, the dichotomy between the coherence of nodal quasiparticles and the incoherence of antinodal ones, which is well established in the normal state, persists in the superconducting state in the underdoped regime. A theoretical analysis using a new sum rule reveals that the superconducting state cannot be described within the standard BCS–Migdal–Eliashberg theory with only one energy scale (the maximum amplitude Δ_m of the superconducting gap): a second energy scale, the slope (v_{Δ}) of the gap at the nodes is needed. We have also established a new relation between the behaviour of the low-energy Raman response and that of the temperature dependence of the superfluid stiffness, both associated with nodal physics. All these observations emphasize the importance of the momentum space differentiation between nodal and antinodal regions in both the normal and superconducting state in the proximity of the Mott transition. The physics of momentum space differentiation can have multiple origins and has been stressed previously by many authors^{37,38}. Modern theoretical approaches, such as cluster perturbation theory, functional renormalization groups, and cluster extensions of dynamical mean-field theory are capable of capturing this physics in the weak coupling and strong coupling regimes of the Hubbard model, respectively^{39–42}. Our results provide further tests for these methods and should stimulate further development of these approaches.

METHODS

DETAILS OF THE EXPERIMENTAL PROCEDURE

The Hg-1201 single crystals have been grown by the flux method. One of the crystal growth procedures that we have developed, as well as Hg-1201's structural and physical properties, are described in ref. 43. The ERS experiments have been carried out using a triple grating spectrometer (JY-T64000) equipped with a nitrogen-cooled charge-coupled device detector. All spectra have been corrected for the spectral response of the spectrometer and for the Bose–Einstein factor. They are thus proportional to the imaginary part of the Raman response function $\chi''(\omega)$. The NR and ANR have been explored using cross polarizations parallel to the Cu–O bond directions (B_{2g}) and at 45° from them (B_{1g}), respectively. Green (2.4 eV) and red (1.9 eV) excitation lines have been used to probe the NR (B_{2g}) and ANR (B_{1g}) Raman response functions, respectively, to reduce the Raman phonon activity and enabled a direct view of the electronic properties of this cuprate without invoking *ad hoc* phonon subtraction procedures usually used in cuprate systems⁴⁴. No sign of resonance by laser excitation lines is detected in the B_{2g}

Raman response functions. Moreover, it has been shown that the B_{2g} background decreases as the doping decreases⁴⁵, so that we can apply the sum rule derived from the t – J model for our B_{2g} data. The spectra presented here have been taken below ($T = 10$ K, corrected for laser heating) and above T_c ($T = 100$ K for 92 K (overdoped), 95 K (optimally doped) 89 K (underdoped) and 86 K (underdoped) crystals, and $T = 89$ K for 78 K (underdoped) and 63 K (underdoped) crystals).

DERIVATION OF EQUATION (2)

The diagrammatic formulation of Fermi-liquid theory isolate, in the diagrammatic expansion for an arbitrary response function, the quasiparticle contributions represented by two electron lines (see below). We apply this formalism, initially introduced by Larkin⁴⁶ and Leggett⁴⁷, to the calculation of the Raman response function χ'' .

$$\chi''(\omega) = \text{Im} [\textcircled{\bullet} + \textcircled{\bullet} + \textcircled{\bullet} + \dots]$$

The shaded elements are irreducible vertices with respect to the quasiparticle lines (BCS electron lines multiplied by an additional QPSW factor of Z relative to the non-interacting case), and do not contain imaginary parts. The quasiparticle contribution is small (linear in ω and T), hence we only keep the second graph (the first one being real, it does not contribute to absorption). This has the form of a non-interacting quasiparticle bubble multiplied by Z^2 , and by a vertex (Λ^2), which describes the renormalization of the Raman tensor via high-energy (non-quasiparticle) processes, leading to equation (2). The higher-order graphs can introduce collective modes at higher energies not considered here.

THEORETICAL SUM RULE

The absolute value of the Raman intensity in samples with different doping levels or composition is difficult to ascertain experimentally, because it depends on geometric factors that are hard to measure, such as the penetration volume of the electromagnetic field into the sample. To circumvent this problem, and to make contact with the physics of the Mott insulator, we use a sum rule to normalize the Raman intensity. In ref. 48, such a sum rule was derived for the Hubbard model. This cannot be used to interpret our experiment however, because it involves the contribution of the Raman intensity from the upper Hubbard band, which cannot be determined experimentally because it occurs at energies where other interband transitions take place. For this reason, we have extended the method of ref. 48 and derived a new low-energy sum rule for the B_{2g} Raman intensity, directly for the t – J model (for which the upper Hubbard band has been projected out). This sum rule relates the low-energy Raman intensity to the expectation value of a composite operator:

$$\int d\omega \omega \chi''(\omega) = \frac{\pi}{2} \langle [M, [H, M^\dagger]] \rangle = \sum_{\substack{ijkl \\ \alpha \dots \delta'}} T_{ijlm}^{\alpha\alpha' \dots \delta\delta'} \\ \times \langle X_{\alpha\alpha'}(i) X_{\beta\beta'}(j) X_{\gamma\gamma'}(l) X_{\delta\delta'}(m) \rangle.$$

In this expression, $X_{\alpha\alpha'}(i)$ is the Hubbard operator at site i , and the Greek indices $\alpha \dots \delta'$ run over the three possible atomic states 0, \uparrow , \downarrow . M is the B_{2g} Raman tensor $M = \sum_{\mathbf{k}\sigma} \sin k_x \sin k_y X_{\sigma 0}(\mathbf{k}) X_{0\sigma}(\mathbf{k})$ and H is the t – J hamiltonian (containing a hopping term and a superexchange interaction). We have calculated the tensor $T_{ijlm}^{\alpha\alpha' \dots \delta\delta'}$ appearing on the right-hand side of this equation. For a hopping term involving nearest (t) and next-nearest neighbour (t'), assuming unbroken spatial and time-reversal symmetry, we have checked that all non-zero contributions involve at least two fermionic operators (that is, $X_{\sigma 0}$ or $X_{0\sigma}$) living on different sites. In the absence of translational symmetry breaking, contributions involving exactly two such operators are proportional to doping. We have checked this from an explicit evaluation using, for example, slave-boson or dynamical mean-field theories. Details will be published elsewhere. Hence, the B_{2g} Raman intensity for the t – t' – J model reads: $\int_0^\infty d\omega \omega \chi''(\omega) = C(t, t', J) p + \dots$ at low doping levels, justifying the normalization used above. A similar observation follows from a different sum rule⁴⁹.

Received 4 March 2006; accepted 28 June 2006; published 23 July 2006.

References

1. Timusk, T. & Statt, B. W. The pseudogap in high-temperature superconductors: an experimental survey. *Rep. Prog. Phys.* **62**, 61–122 (1999).
2. Devereaux, T. P. & Einzel, D. Electronic Raman scattering in superconductors as a probe of anisotropic electron pairing. *Phys. Rev. B* **51**, 16336–16357 (1995).

3. Venturini, F. *et al.* Doping dependence of the electronic Raman spectra in cuprates. *J. Phys. Chem. Solids* **63**, 2345–2349 (2002).
4. Sugai, S., Suzuki, H., Takayanagi, Y., Hosokawa, T. & Hayamizu, N. Carrier-density-dependent momentum shift of the coherent peak and the LO phonon mode in p-type high- T_c superconductors. *Phys. Rev. B* **68**, 184504 (2003).
5. Chen, X. K. *et al.* Electronic Raman scattering in underdoped $\text{YBa}_2\text{Cu}_3\text{O}_{8.5}$. *Phys. Rev. B* **56**, R513–R516 (1997).
6. Presland, M. R., Tallon, J. L., Buckley, R. G., Liu, R. S. & Flower, N. E. General trends in oxygen stoichiometry effects on T_c in Bi and Tl superconductors. *Physica C* **176**, 95–105 (1991).
7. Chubukov, A. V., Devereaux, T. P. & Klein, M. V. Resonance mode in B_{1g} Raman scattering: A way to distinguish between spin-fluctuation and phonon-mediated d-wave superconductivity. *Phys. Rev. B* **73**, 094512 (2006).
8. Klein, M. V. & Dierker, S. B. Theory of Raman scattering in superconductors. *Phys. Rev. B* **29**, 4976–4991 (1984).
9. Hewitt, K. C. & Irwin, J. C. Doping dependence of the superconducting gap in $\text{Bi}_2\text{Sr}_2\text{CaCu}_2\text{O}_{8-\delta}$. *Phys. Rev. B* **66**, 054516 (2002).
10. Bonn, D. A. *et al.* Surface impedance studies of YBCO. *Czech. J. Phys.* **46**, 3195–3202 (1996).
11. Panagopoulos, C. & Xiang, T. Relationship between the superconducting energy gap and the critical temperature in high- T_c superconductors. *Phys. Rev. Lett.* **81**, 2336–2339 (1998).
12. Lee, P. A. & Wen, X. G. Unusual superconducting state of underdoped cuprates. *Phys. Rev. Lett.* **78**, 4111–4114 (1997).
13. Wen, X. G. & Lee, P. A. Theory of quasiparticles in the underdoped high- T_c superconducting state. *Phys. Rev. Lett.* **80**, 2193–2196 (1998).
14. Ioffe, L. B. & Millis, A. J. d-wave superconductivity in doped Mott insulators. *J. Phys. Chem. Solids* **63**, 1196–1198 (1987).
15. Broun, D. M. *et al.* Superfluid density reveals a quantum critical point between d-wave superconductivity and a Mott insulator. Preprint at <<http://arxiv.org/cond-mat/0509223>> (2005).
16. Anderson, P. W. The resonating valence bond state in La_2CuO_4 and superconductivity. *Science* **235**, 1196–1198 (1987).
17. Kotliar, G. & Liu, J. The superexchange mechanism and d-wave superconductivity. *Phys. Rev. B* **38**, 5142–5145 (1988).
18. Gros, C. Superconductivity in correlated wave functions. *Phys. Rev. B* **38**, 931–934 (1988).
19. Anderson, P. W. *et al.* The physics behind high-temperature superconducting cuprates: the plain vanilla version of RVB. *J. Phys. Condens. Matter* **16**, R755–R769 (2004).
20. Yoshida, T. *et al.* Metallic behavior of lightly doped $\text{La}_{2-x}\text{Sr}_x\text{CuO}_4$ with a Fermi surface forming an arc. *Phys. Rev. Lett.* **91**, 027001 (2003).
21. Shen, K. M. *et al.* Nodal quasiparticles and antinodal charge ordering in $\text{Ca}_{2-x}\text{Na}_x\text{CuO}_2\text{Cl}_2$. *Science* **307**, 901–904 (2005).
22. Mesot, J. *et al.* Superconducting gap anisotropy and quasiparticle interaction: A doping dependent photoemission study. *Phys. Rev. Lett.* **83**, 840–843 (1999).
23. Borisenko, S. V. *et al.* Superconducting gap in the presence of bilayer splitting in underdoped $(\text{Pb}, \text{Bi})_2\text{Sr}_2\text{CaCu}_2\text{O}_{8-\delta}$. *Phys. Rev. B* **66**, 140509(R) (2002).
24. Norman, M. R. *et al.* Destruction of the Fermi surface in underdoped high- T_c superconductors. *Nature* **392**, 157–160 (1998).
25. Benfatto, L., Caprara, S. & Di Castro, C. Gap and pseudogap evolution within the charge-ordering scenario for superconducting cuprates. *Eur. Phys. J. B* **17**, 95–102 (2000).
26. Chakravarty, S., Laughlin, R. B., Morr, D. K. & Nayak, C. Hidden order in the cuprates. *Phys. Rev. B* **63**, 094503 (2001).
27. Won, H., Haas, S., Parker, D. & Maki, K. High- T_c cuprate superconductivity in a nutshell. *Phys. Status Solidi B* **242**, 363–369 (2005).
28. Campuzano, J. C. *et al.* Electronic spectra and their relation to the (π, π) collective mode in high- T_c superconductors. *Phys. Rev. Lett.* **83**, 3709–3712 (1999).
29. Ding, H. *et al.* Coherent quasiparticle weight and its connection to high- T_c superconductivity from angle-resolved photoemission. *Phys. Rev. Lett.* **87**, 227001 (2001).
30. Sutherland, M. *et al.* Thermal conductivity across the phase diagram of cuprates: Low-energy quasiparticles and doping dependence of the superconducting gap. *Phys. Rev. B* **67**, 174520 (2003).
31. McElroy, K. *et al.* Coincidence of checkerboard charge order and antinodal state decoherence in strongly underdoped superconducting $\text{Bi}_2\text{Sr}_2\text{CaCu}_2\text{O}_{8+\delta}$. *Phys. Rev. Lett.* **94**, 197005 (2005).
32. Miyakawa, N., Guptasarma, P., Zasadzinski, J. F., Hinks, D. G. & Gray, K. E. Strong dependence of the superconducting gap on oxygen doping from tunneling measurements on $\text{Bi}_2\text{Sr}_2\text{CaCu}_2\text{O}_{8-\delta}$. *Phys. Rev. Lett.* **80**, 157–160 (1998).
33. Miyakawa, N. *et al.* Predominantly superconducting origin of large energy gaps in underdoped $\text{Bi}_2\text{Sr}_2\text{CaCu}_2\text{O}_{8-\delta}$ from tunneling spectroscopy. *Phys. Rev. Lett.* **83**, 1018–1021 (1999).
34. DeWilde, Y. *et al.* Unusual strong-coupling effects in the tunneling spectroscopy of optimally doped and overdoped $\text{Bi}_2\text{Sr}_2\text{CaCu}_2\text{O}_{8-\delta}$. *Phys. Rev. Lett.* **80**, 153–156 (1998).
35. Hoffman, J. E. *et al.* Imaging quasiparticle interference in $\text{Bi}_2\text{Sr}_2\text{CaCu}_2\text{O}_{8+\delta}$. *Science* **297**, 1148–1151 (2002).
36. Deutscher, G. Coherence and single-particle excitations in the high-temperature superconductors. *Nature* **397**, 410–412 (1999).
37. Stojkovic, B. P. & Pines, D. Theory of the longitudinal and Hall conductivities of the cuprate superconductors. *Phys. Rev. B* **55**, 8576–8595 (1997).
38. Ioffe, L. B. & Millis, A. J. Zone-diagonal-dominated transport in high- T_c cuprates. *Phys. Rev. B* **58**, 11631–11637 (1998).
39. Honerkamp, C., Salmhofer, M., Furukawa, N. & Rice, T. M. Breakdown of the Landau–Fermi liquid in two dimensions due to umklapp scattering. *Phys. Rev. B* **63**, 035109 (2001).
40. Katanin, A. A. & Kampf, A. P. Quasiparticle anisotropy and pseudogap formation from the weak-coupling renormalization group point of view. *Phys. Rev. Lett.* **93**, 106406 (2004).
41. Civelli, M., Capone, M., Kancharla, S. S., Parcollet, O. & Kotliar, G. Dynamical breakup of the Fermi surface in a doped mott insulator. *Phys. Rev. Lett.* **95**, 106402 (2005).
42. S n chal, D. & Tremblay, A. M. S. Hot spots and pseudogaps for hole- and electron-doped high-temperature superconductors. *Phys. Rev. Lett.* **92**, 126401 (2004).
43. Bertinotti, A. *et al.* in *Studies of High Temperature Superconductors* Vol. 23 (ed. Narlikar, A.) 27–85 (Nova Science Publishers, New York, 1997).
44. Le Tacon, M., Sacuto, A. & Colson, D. Two distinct electronic contributions in the fully symmetric Raman response of high T_c cuprates. *Phys. Rev. B* **71**, 100504(R) (2005).
45. Opel, M. *et al.* Carrier relaxation, pseudogap, and superconducting gap in high- T_c cuprates: A Raman scattering study. *Phys. Rev. B* **61**, 9752–9844 (2000).
46. Larkin, A. I. Effect of collective excitations on the electrodynamics of superconductors. *Sov. Phys. JETP* **19**, 1478–1486 (1964).
47. Leggett, A. J. Theory of a superfluid Fermi liquid. I. General formalism and static properties. *Phys. Rev.* **140**, A1869–A1888 (1965).
48. Freericks, J. K., Devereaux, T. P., Moraghebi, M. & Cooper, S. L. Optical sum rules that relate to the potential energy of strongly correlated systems. *Phys. Rev. Lett.* **94**, 216401 (2005).
49. Shastry, S. & Shraiman, B. Theory of Raman scattering in Mott–Hubbard systems. *Phys. Rev. Lett.* **65**, 1068–1071 (1990).

Acknowledgements

We are grateful to S. Biermann, N. Bontemps, S.V. Borisenko, P. Bourges, M. Cazayous, R. Combescot, L. de Medici, T.P. Devereaux, K. McElroy, P. Monod, M. Norman, Z.-X. Shen, and L. Taillefer for useful discussions. This research was supported by CNRS, Ecole Polytechnique and the ‘Chaire Blaise Pascal de la Fondation de l’Ecole Normale Sup rieure et de la r gion Ile de France’. Correspondence and requests for materials should be addressed to M.L.T.

Competing financial interests

The authors declare that they have no competing financial interests.

Reprints and permission information is available online at <http://npg.nature.com/reprintsandpermissions/>